Solving the one-dimensional penetration problem for the fission channel in the statistical Hauser-Feshbach theory

T. Kawano,[1,*] P. Talou,[1,†] and S. Hilaire[2,3]
[1]*Los Alamos National Laboratory, Los Alamos, New Mexico 87545, USA*
[2]*CEA, DAM, DIF, F-91297 Arpajon, France*
[3]*Université Paris-Saclay, CEA, LMCE, F-91680 Bruyères-le-Châtel, France*

(Received 1 July 2023; revised 16 January 2024; accepted 8 March 2024; published 9 April 2024)

We solve the Schrödinger equation for an arbitrary one-dimensional potential energy to calculate the transmission coefficient in the fission channel of compound nucleus reactions. We incorporate the calculated transmission coefficients into the statistical Hauser-Feshbach model calculation for neutron-induced reactions on ^{235,238}U and ^{239}Pu. The one-dimensional model reproduces the evaluated fission cross section data reasonably well considering the limited number of model parameters involved. A resonance-like structure appears in the transmission coefficient for a double-humped fission barrier shape that includes an intermediate well, which is understood to be a quantum mechanical effect in the fission channel. The calculated fission cross sections for the neutron-induced reactions on ^{235,238}U and ^{239}Pu all exhibit a similar structure.

DOI: 10.1103/PhysRevC.109.044610

I. INTRODUCTION

The statistical compound nucleus theory describes the probability for a formed compound nucleus to decay into a channel a by the partial width Γ_a, and the Hauser-Feshbach theory [1] tells us that the energy-average of width $\langle \Gamma_a \rangle$ can be replaced by the optical model transmission coefficient T_a in the time-reverse process. This is intuitive for particle or photon-induced reactions, as the interpretation is that the strength to decay into the channel a is proportional to the compound nucleus formation probability from the same channel. For the fission channel, however, the reverse process is not at all trivial. Several approximations and models are then employed, which significantly complicate the comparison and interpretation with experimental fission cross-section data. Studies on the nuclear fission have a long history, and comprehensive review articles of the fission calculation are given by Bjørnholm and Lynn [2], Wagemans [3], and more recently Talou and Vogt [4].

A traditional approach to calculate the fission penetrability (transmission coefficient) in the existing Hauser-Feshbach codes is to first assume an inverted parabola for a single fission barrier, and solve a penetrability by adopting the semiclassical Wentzel-Kramers-Brillouin (WKB) approximation [2,5], which is often called the Hill-Wheeler penetrability. We often assume that one-dimensional (1-D) potential energy forms a double-humped fission barrier shape, which is predicted by the liquid drop model with the microscopic (shell and pairing energies) corrections. By decoupling these two fission barriers, and calculating each Hill-Wheeler penetrability separately, an effective (net) transmission coefficient T_f through the whole potential energy is calculated as

$$T_f = \frac{T_A T_B}{T_A + T_B}, \tag{1}$$

where T_A and T_B are the Hill-Wheeler penetrability through the barriers given in Sec. II. Obviously this treatment oversimplifies the fission penetration problem, as it ignores the potential wells between barriers which gives rise to the so-called class-II and class-III (in the triple-humped case) states. By introducing the average spacing of the class-II states D_{II}, the penetration probabilities through the different barriers are coupled [6–8] to calculate the net fission probability. Bouland, Lynn, and Talou [9] implemented the transition states in the class-II well, through which the penetrability is expressed in terms of the R-matrix formalism. Bhandari [10] and Sin *et al.* [11,12] defined a continuous fission barrier shape and applied WKB for each segment to calculate the effective transmission coefficient. Romain, Morillon, and Duarte [13] reported an antiresonant transmission due to the class-II and class-III states. Some recent developments in the fission calculations are summarized in Ref. [4] and references therein.

Segmentation of the potential energy along the nuclear elongation axis, where the inner barrier, class-II state, outer barrier, class-III states, etc., are aligned along the deformation coordinate, is convenient to calculate the penetration through the entire potential energy surface. Often we calculate the penetration for each of the segments separately, and combine them. Within such an approximation, however, the quantum-mechanical tunneling disappears, because the wave function of the entire system is not considered. Although limited to an analytical expression of potential energy, Cramer and Nix [14] obtained an exact solution for this wave function in terms of the parabolic-cylinder functions for the

*kawano@lanl.gov
†patrick.talou@gmail.com

double-humped potential shape. Sharma and Leboeuf [15] extended this technique to the triple-humped potential barrier case. By solving the Schrödinger equation numerically, an extension of the Cramer-Nix model to an arbitrary shape of 1-D potential energy is straightforward. This was reported by Morillon, Duarte, and Romain [16] and by ourselves [17], where the effective transmission coefficient in Eq. (1) is no longer involved. The solution of Schrödinger equation for 1-D potential is, however, just one of all the possible fission paths, whereas the dynamical fission process takes place through any excited states on top of the fission barrier. To calculate the actual fission transmission coefficient that can be used in the Hauser-Feshbach theory calculations, we have to take into account the penetration through the barriers corresponding to the excited states as well.

Eventually we describe the nuclear fission process from two extreme point of views, namely that the compound nucleus evolves through a fixed albeit large number of fission paths, or that the configuration is fully mixed in the potential well so that the penetration through the multiple barriers can be totally decoupled. In the decoupled limit, we can assume that another semistable compound nucleus is produced, which has various excitation energies. This nucleus is formed by the probability of T_A, and decays just like the first compound nucleus; it may emit a neutron or γ rays, or go beyond the second fission barrier with the probability T_B. This approach is similar to the traditional models, although it may require a substantial change in the multistage Hauser-Feshbach algorithm.

Our approach follows the former case; the fission process takes place along an eigenstate of the compound nucleus, which is continuous along the nuclear deformation coordinate. By introducing a probability of forming the semistable compound nucleus besides the fission penetration, we are able to consider situations somewhere in between two scenarios. However, this is beyond the scope of the current study, and we hold it for future development. In this paper, we revisit the Cramer-Nix model and its extension to the arbitrary potential energy shape, and introduce nuclear excitation to calculate the effective transmission coefficient T_f. The obtained T_f is used in the Hauser-Feshbach theory to calculate the fission cross section, which can be compared with available experimental data. We perform the cross-section calculations for two distinct physical cases corresponding to fertile and fissile targets: the neutron-induced fission on ^{238}U where the total excitation energy is still under the fission barrier, and that for ^{235}U and ^{239}Pu where the system energy is higher than the barrier. In this paper we limit ourselves to the first-chance fission only, where no neutron emission occurs prior to fission. However, extension to the multichance fission process is not complicated at all.

II. THEORY

A. Fission transmission coefficient for double-humped fission barrier

First we briefly summarize the standard technique to calculate the fission transmission coefficient T_f for the double-humped fission barrier. The objective is to emphasize the

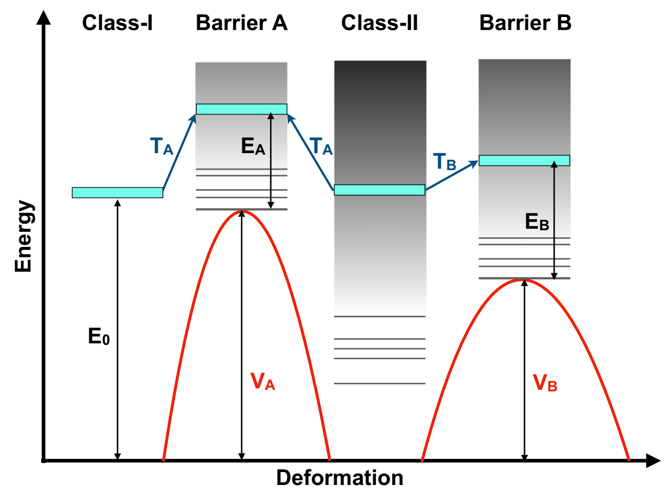

FIG. 1. Schematic picture of double-humped potential energy along the nuclear deformation direction, showing the double-humped fission barriers V_A and V_B, and the class-I and class-II wells between the barriers. The initial compound nucleus state is at E_0 in class I, which decays through the states at E_A and E_B on top of each barrier.

distinction between the conventional fission calculation and our approach. Traditionally The fission barrier is approximated by an inverted parabola characterized by the barrier parameters: the heights V_A for the inner barrier and V_B for the outer barrier, and their curvatures C_A and C_B (the curvature is also denoted by $\hbar\omega$), as shown schematically in Fig. 1. By applying the WKB approximation to the parabolic-shaped barriers, the transmission coefficient is given by the Hill-Wheeler expression [5]

$$T_i(E) = \frac{1}{1 + \exp\left(2\pi \frac{V_i + E - E_0}{C_i}\right)}, \quad i = A, B, \tag{2}$$

where E_0 is the initial excitation energy and E are the nuclear excitation energies measured from the top of each barrier. For a neutron-induced fission case, $E_0 = E_n + S_n$, where E_n is the incident neutron energy in the center-of-mass system, and S_n is the neutron separation energy. The fission transmission coefficient $T^{J\Pi}$ for the compound nucleus spin J and parity Π is the sum of all penetrabilities through the barriers corresponding to the excited states at $E = E_k$ for the discrete levels and at $E = E_x$ in the continuum with the same spin and parity:

$$T_i^{J\Pi} = \sum_k T_i(E_k)\delta_{J_k,J}\delta_{\Pi_k,\Pi} + \int_{E_{c,i}}^{\infty} T_i(E_x)\rho_i(E_x, J, \Pi)dE_x, \quad i = A, B, \tag{3}$$

where $\rho(E_x, J, \Pi)$ is the level density on top of each barrier, E_c is the highest discrete state energy, and the Kronecker deltas ensure that the spin and parity of the kth discrete state are the same as J and Π. This implies that the barrier associated with each excited state is obtained by simply shifting the ground-state barrier by the excitation energy. Often some phenomenological models are applied to $\rho(E_x, J, \Pi)$ to take the nuclear deformation effect into account, which is the so-called collective enhancement [18]. A standard technique in calculating fission cross sections, *e.g.* as adopted by Iwamoto [19], assumes typical nuclear deformations at the inner and outer barriers. Although the collective enhancement is a consequence of change in the nuclear shape and structure, it is model and assumption-dependent in general, which makes fission model comparison difficult.

When the fission barriers V_A and V_B are fully decoupled, $T_A^{J\Pi}$ represents a probability of going through the inner barrier, and a branching ratio from the intermediate state to the outer direction is $T_B^{J\Pi}/(T_A^{J\Pi}+T_B^{J\Pi})$ for a given $J\Pi$. The effective fission transmission coefficient is thus given by Eq. (1). This expression implies that the dynamical process in the class-II well is fully adiabatic, and it virtually forms another compound state. It should be noted that there is no explicit fission path in this model, since integration over the excited states in Eq. (3) is performed before connecting $T_A^{J\Pi}$ and $T_B^{J\Pi}$.

In the following subsections, we define T_f in another way. To distinguish the standard fission transmission coefficient defined by Eqs. (1)–(3), which is generally employed by statistical Hauser-Feshbach nuclear reaction codes, we denote the conventional T_f in Eq. (1) by $T_f^{\rm STD}$ in our discussions, unless otherwise specified.

B. Fission transmission coefficient for 1-D shape

1. Concatenated parabolas

The Schrödinger equation for an arbitrary one-dimensional (1-D) potential energy shape can be solved exactly without the WKB approximation by applying the numerical integration technique. Although our purpose is to solve problems for any fission barrier shape, it is still convenient to employ the parabolic representation to compare with the two inverted parabola cases. Similar to the three-quadratic-surface parametrization of nuclear shape [20,21], the 1-D barrier is parametrized by smoothly connected parabolas

$$V(i,x) = V_i + (-1)^i \tfrac{1}{2} c_i (x-x_i)^2, \quad i = 1,2,\ldots, \tag{4}$$

where i is the region index for the segmented parabola (odd i for barriers, and even for wells), x is a dimensionless deformation coordinate, $c_i = \mu C_i^2/\hbar^2$, V_i is the top (bottom) energy of the barrier (well), x_i is the center of each parabola, and μ is the inertial mass parameter. Note that the region index adopted here corresponds to the double-humped case if $A = 1$ and $B = 3$. Because the deformation coordinate is dimensionless, the calculated result is insensitive to μ, and we take

$$\frac{\mu}{\hbar^2} = 0.054 A^{5/3}\ \mathrm{MeV}^{-1} \tag{5}$$

as suggested by Cramer and Nix [14]. The region index i runs from 1 to 3 for the double-humped shape, and from 1 to 5 for the triple-humped shape. The double-humped case is shown in Fig. 2 by the solid curve.

By providing the barrier parameters V_i and C_i, the junction point (ξ_i) and the parabola center (x_i) for each adjacent region are automatically determined through continuity relations. Since the abscissa is arbitrary in the 1-D model, we first fix

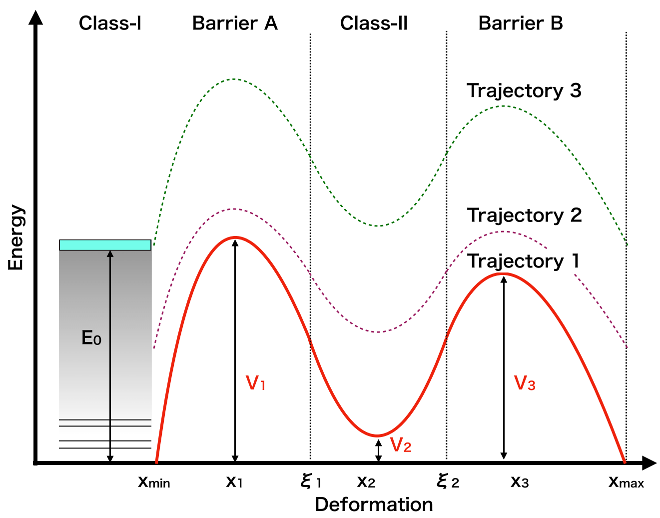

FIG. 2. Schematic picture of 1-D potential energy along the nuclear deformation direction. The initial compound nucleus state is at E_0, which decays through 1-D fission paths, e.g., the trajectories 1, 2, etc.

the center of the first barrier at

$$x_1 = x_{\rm min} + \sqrt{\frac{2V_1}{c_1}}, \tag{6}$$

where $x_{\rm min}$ is an arbitrary small offset. The consecutive central points are given by

$$x_i = x_{i-1} + \sqrt{\frac{2|V_{i-1}-V_i|(c_{i-1}+c_i)}{c_{i-1}c_i}}, \tag{7}$$

and the junction points are

$$\xi_i = \frac{c_i x_i + c_{i+1}x_{i+1}}{c_i + c_{i+1}}. \tag{8}$$

With the central points of Eq. (7) and the junction points of Eq. (8), the segmented parabolas in Eq. (4) are smoothly concatenated.

2. Solution of 1-D Schrödinger equation

The 1-D Schrödinger equation for the fission channel of a compound nucleus at the system energy E is written as [14]

$$\frac{d^2}{dx^2}\phi(x) + \frac{2\mu}{\hbar^2}\{E - [V(x) + iW(x)]\}\phi(x) = 0, \tag{9}$$

where the wave function $\phi(x)$ satisfies the following boundary condition [22]:

$$\phi(x) \simeq \begin{cases} u^{(-)}(kx) - S u^{(+)}(kx), & x > x_{\rm max}, \\ A u^{(-)}(kx), & x < x_{\rm min}. \end{cases} \tag{10}$$

$[x_{\rm min}, x_{\rm max}]$ is the entire range of fission barrier considered, $k = \sqrt{2\mu E}$ is the wave number, A is the amplitude of the wave function in the class-I well, and

$$u^{(\pm)}(kx) = \cos(kx) \pm i \sin(kx). \tag{11}$$

The Schödinger equation in the internal region can be solved numerically by a standard technique such as the Numerov method or Fox-Goodwin method [23]. The solution at the matching point x_m in the external region ($x_m > x_{\max}$) is written as

$$\psi(x_m) = u^{(-)}(kx_m) - Su^{(+)}(kx_m), \tag{12}$$

and the internal solution $\phi(x_m)$ is smoothly connected with the external solution at x_m. Analogously to the scattering matrix element in the single-channel optical model, the coefficient S is then given by

$$S = \frac{fu^{(-)}(x_m) - g^{(-)}}{fu^{(+)}(x_m) - g^{(+)}}, \tag{13}$$

where

$$f \equiv \left.\frac{d\phi/dx}{\phi}\right|_{x_m} \quad \text{and} \quad g^{(\pm)} \equiv \left.\frac{du^{(\pm)}}{dx}\right|_{x_m}. \tag{14}$$

When the potential is real everywhere, the fission transmission coefficient is given by

$$T = 1 - |S|^2. \tag{15}$$

It is possible to add a small imaginary potential that accounts for flux absorption [12] in the class-II and/or class-III well between the barriers. In the case of the complex potential, the amplitude A in Eq. (10) is given by the normalization factor of the internal wave function at x_m,

$$A = \left.\frac{u^{(-)} - Su^{(+)}}{\phi}\right|_{x_m}, \tag{16}$$

and the transmission coefficient through the barrier is $T_d = |A|^2$. Because of the loss of flux due to the imaginary potential, T_d is smaller than T, and T_d goes into the statistical Hauser-Feshbach theory instead of T. Similarly to the optical model, the lost flux gives a probability of forming another CN, and this CN initiates further decay chains through the fission and γ-ray emission channels. The neutron emission channel may open when its excitation energy is still larger than the neutron separation energy. Although such calculation is feasible, we aim at demonstrating the main feature of current modeling in contrast to the T_f^{STD} calculation in the real potential case. In the following discussion, the potential is always real.

3. Potential energy for excited states

Since penetration through the potential defined by Eq. (4) is merely one of all the possible fission paths, we have to aggregate such possible trajectories (paths) to calculate the summed transmission coefficient, which is analogous to Eq. (3). While the fission penetration for the ground state takes place through the shape of potential energy in Eq. (4), each of the excited states would be constructed on top of the ground state trajectory. This is a critical difference between the T_f^{STD} calculation and 1-D model, as an adiabatic intermediate state assumed in the conventional model conceals an actual fission path along the deformation coordinate, while it is explicit in the 1-D model.

To define the fission trajectories for the excited states, one of the most naive assumptions, like Eq. (2) being summed in Eq. (3) by shifting the excitation energy, is that the potential energy is shifted by the excitation energy E_x as $V(x) = V_0(x) + E_x$, where V_0 is the potential for the ground state. This, however, ignores distortion of the eigenstate spectrum in a compound nucleus whose shape changes. At the limit of adiabatic change in the nuclear shape, the excitation energy of each of the eigenstates changes slightly due to shell, pairing, and nuclear deformation effects. It is in particular well known that the moment of inertia of a nucleus increases with deformation, which reduces the spacing between the levels within a rotational band. This results in distortion of the trajectories, as opposed to a simple shift in energy.

We empirically know that calculated fission cross sections underestimate experimental data if we simply adopt the level density $\rho(E_x)$ for the ground state deformation in the sum of Eq. (3). Therefore we often employ some models to enhance the level densities on top of each of the barriers, which account for increasing collective degree-of-freedom in a strongly deformed nucleus. Instead of introducing the collective enhancement in our 1-D penetration calculation, we assume the excitation energies of the states will be lowered due to the nuclear deformation. In other words, the eigenstates in a compound nucleus at relatively low excitation energies are distorted by deformation effects. An illustration of the distortion effect corresponding to a compression is schematically shown in Fig. 2 by the dotted curves: trajectories 2 and 3. These trajectories are defined for all the discrete levels and for all continuum bins in the compound nucleus, which maintains the band structure of collective states along the nuclear deformation coordinate. For example, the ground-state rotational band is seen at any deformation points.

The trajectory compression should be mitigated for the higher excitation energies, which is also phenomenologically known as the damping of collectivity. Although the compression might depend on the deformation as it changes the pairing and shell effects, we model the compression in a rather simple way to eliminate unphysical overfitting to observed data. We assume the eigenstates in the compound nucleus are compressed by a factor that depends on the excitation energy only. Our ansatz reads

$$\varepsilon_x = \{f_0 + (1 - e^{-f_1 E_x})(1 - f_0)\}E_x, \tag{17}$$

where the parameter f_0 is roughly 0.8 and the damping f_1 is $\approx$0.2 MeV^{-1} as shown later. The corresponding fission trajectory for the excited states is now

$$V(x) = V_0(x) + \varepsilon_x. \tag{18}$$

Because the discrete level representation and the level density for the target nucleus are smoothly connected at E_c, Eqs. (17) and (18) ensure this smoothness everywhere in the trajectory. The transmission coefficient for this trajectory is $T(\varepsilon_x)$, and the fission transmission coefficient $T_f^{J\Pi}$ is given by

$$T_f^{J\Pi} = \sum_k T(\varepsilon_k)\delta_{J_k,J}\delta_{\Pi_k,\Pi} + \int_{E_c}^{\infty} T(\varepsilon_x)\rho(\varepsilon_x, J, \Pi)dE_x. \tag{19}$$

Although the integration range goes to infinity, or some upper-limit value could be considered [24], this converges quickly

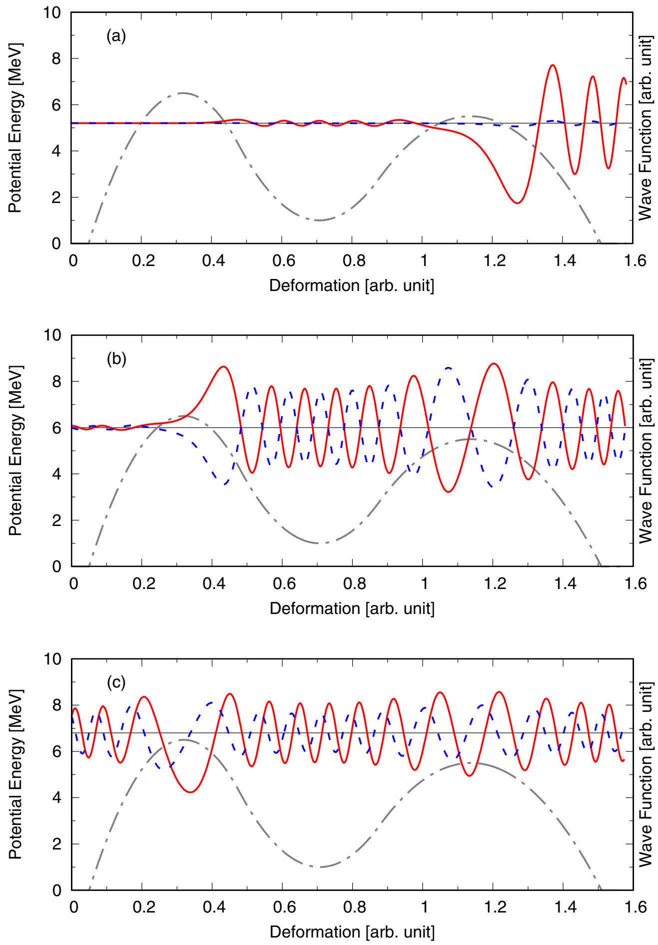

FIG. 3. Calculated wave functions for the connected parabolas. The potential energy is shown by the dot-dashed curves. The solid and dotted curves are the normalized wave function (solid for the real part, and dotted for the imaginary part). (a) The system energy lies below both barrier heights, (b) the energy is between the barriers, and (c) it is above the barriers.

with increasing excitation energy. Generally it is safe to truncate the integration at $E_x = E_0$.

III. RESULTS AND DISCUSSION

A. Wave function and transmission coefficient for a single fission path

As an example of the 1-D model, the calculated wave functions for connected parabolas are shown in Fig. 3, which is for the $A = 239$ system. The assumed barrier heights are $V_1 = 6.5$, $V_2 = 1$, and $V_3 = 5.5$ MeV, with the curvatures of $C_1 = 0.6$, $C_2 = 0.4$, and $C_3 = 0.5$ MeV. We depict the three cases of system energy E: (a) below both of the barriers, (b) between V_1 and V_3, and (c) above both.

Since the 1-D potential penetration problem is invariant whether numerical integration is performed from the right or left side, the wave function is normalized to the external function that has unit amplitude. The penetrability is seen as the amplitude of the wave function inside the potential region. Apparently the wave function penetrates through the potential barrier when the system has enough energy to overcome the both barriers $E > V_1$ and $E > V_3$, and it is blocked if the barrier is higher than the system energy. However, although the wave function damps rapidly, quantum tunneling is still seen beyond the barrier.

One of the remarkable differences from $T_f^{\rm STD}$ is that the 1-D model sometimes exhibits resonating behavior due to the penetration through the class-II well. This was already reported by Cramer and Nix [14] in their parabolic-cylinder function expression. It should be noted that this is not an actual compound nucleus resonance, but a sort of the size effect where the traveling and reflecting waves have accidentally the same phase. As a result the wave function is amplified significantly at a resonating energy.

This amplification can be seen easily in the transmission coefficient in Fig. 4. The top panel is for the same potential as the one in Fig. 3. The first sharp resonance appears below the inner barrier of $V_1 = 5.5$ MeV, and the second broader resonance is just above the barrier. We also depicted the transmission coefficients, T_1, and T_2, calculated with the WKB approximation in Eq. (2) for the inner (V_1) and outer (V_3) barriers. When we combine these two fission transmission coefficients by Eq. (1) in the case for Fig. 4(a), the effective fission transmission coefficient becomes almost the same as T_1 at low energies, because $T_1 \ll T_3$ [we do not show $T_1T_3/(T_1 + T_3)$, since it overlaps with T_1 except for in the region $T_1 \simeq 1$]. $T_1T_3/(T_1 + T_3) \simeq T_1$ agrees with the 1-D model in the energy range above 5.8 MeV. However, it deviates notably from the 1-D model when an interference effect of penetrations through the inner and outer barriers becomes visible.

This effect becomes more remarkable when the inner and outer barriers have a similar magnitude, which results in a special circumstance that the penetration and reflection waves are in phase. The bottom panel in Fig. 4 is the case where these barriers have the same height of 6.0 MeV. A broad resonance appears just below the fission barrier, which enhances the fission cross section even if the compound state is still below the fission barrier. Then the penetration drops rapidly as the excitation energy decreases. In contrast, the transmission coefficients T_1 and T_3 by WKB for the inner and outer barriers stay higher in the subthreshold region. The combined transmission coefficient $T_1T_3/(T_1 + T_3)$ is slightly lower than T_3 but almost identical below 5.6 MeV. Under these circumstances, the standard technique of fission calculation using $T_f^{\rm STD}$ may give unreliable fission cross sections in the subthreshold region, albeit these cross sections are very small and experimental data might be uncertain. Nuclear reaction codes sometimes introduce a phenomenological class-II (and class-III) resonance effect to compensate for this deficiency [4,25].

The difference in the WKB curves in Fig. 4(b) is due to the curvatures, and both curves approach $T_A = T_B = 1$ once the system has more than the barrier energy. However, the effective transmission coefficient becomes $1/2$ when Eq. (1) is applied. This is also an important difference between T_f and $T_f^{\rm STD}$, as the 1-D model always gives $T = 1$ when the system energy can overcome all the barriers.

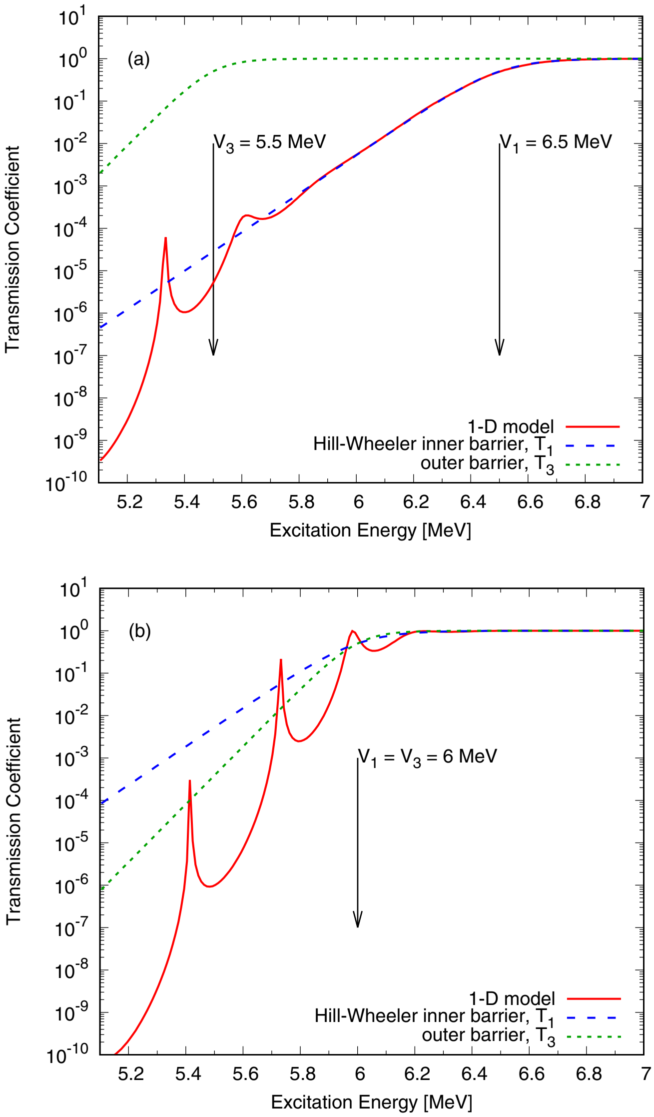

FIG. 4. Calculated transmission coefficients for the connected parabolas as a function of the excitation energy. The top panel (a) is for the potential characterized by $V_1 = 6.5$, $V_2 = 1.0$, and $V_3 = 5.5$ MeV, with the curvatures of $C_1 = 0.6$, $C_2 = 0.4$, and $C_3 = 0.5$ MeV, and the bottom panel (b) is for the $V_1 = V_3 = 6.0$ MeV case. The dashed and dotted curves are the WKB approximations for the inner and outer barriers.

B. Hauser-Feshbach model calculation

We incorporate the fission transmission coefficient in Eq. (19) into the statistical Hauser-Feshbach model calculation to demonstrate applicability of the 1-D model in actual compound nucleus calculations.

The calculation is performed with the $\mathrm{CoH_3}$ statistical Hauser-Feshbach code [26], which properly combines the coupled-channels optical model and the statistical Hauser-Feshbach theory by performing the Engelbrecht-Weidenmüller transformation [27–29] of the optical model penetration matrix [30]. This is particularly important for nuclear reaction modeling in the actinide mass region. We employ the coupled-channels optical potential by Soukhovitskii

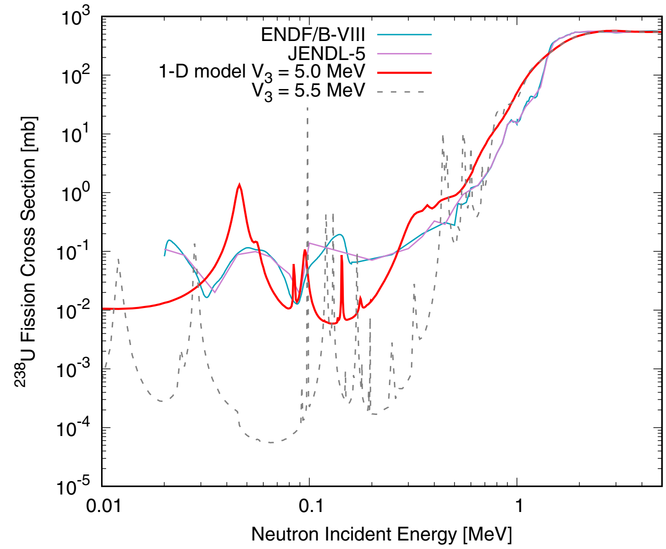

FIG. 5. Calculated fission cross section for neutron-induced reaction on ^{238}U. The barrier height parameters are $V_1 = 6.0$, $V_2 = 0.5$, and $V_3 = 5.0$ for the solid curve. The dashed curve is for $V_3 = 5.5$ MeV.

et al. [31] for producing the neutron penetration matrix and the generalized transmission coefficients [32].

To look at the fission channel more carefully, we take some reasonable model inputs for other reaction channels from literature and do not attempt to fine tune, as the purpose of this study is not a parameter fitting. Since the curvature parameters C are relatively insensitive to fitting fission cross section calculation, we fix them to a typical value of 0.6 MeV, and roughly estimate the heights of inner and outer barriers as well as the trajectory compression parameters in Eq. (17) by comparing with experimental fission cross section data. The class-II depth has also a moderate impact on the calculation of transmission coefficients as far as we provide a reasonable value. We fix it to 0.5 MeV. Other model parameters are set to default internal values in $\mathrm{CoH_3}$. The γ-ray strength function is taken from Kopecky and Uhl [33] with the $M1$ scissors mode [34], the level density is from the Gilbert-Cameron composite formula [35,36], and the discrete level data are taken from RIPL-3 [37].

First, we perform the statistical model calculations for neutron-induced reaction on ^{238}U, where subthreshold fission may be seen below about 1 MeV of incident neutron energy. The ground state rotational band members, 0^+, 2^+, 4^+, and 6^+, are coupled with the deformation parameters taken from the finite range droplet model (FRDM) [38]. The calculated fission cross sections are shown in Fig. 5 by comparing with the evaluated fission cross sections in ENDF/B-VIII.0 [39] and JENDL-5 [40]. The reason for showing the evaluations instead of actual experimental data is that the evaluated data often include more experimental information than the direct measurement of ^{238}U fission cross section, e.g., cross section ratio measurements. The accuracy of the evaluations is good enough to test the relevance of this new model. We found that the case of $V_1 = 6$, $V_2 = 0.5$, and $V_3 = 5$ MeV reasonably

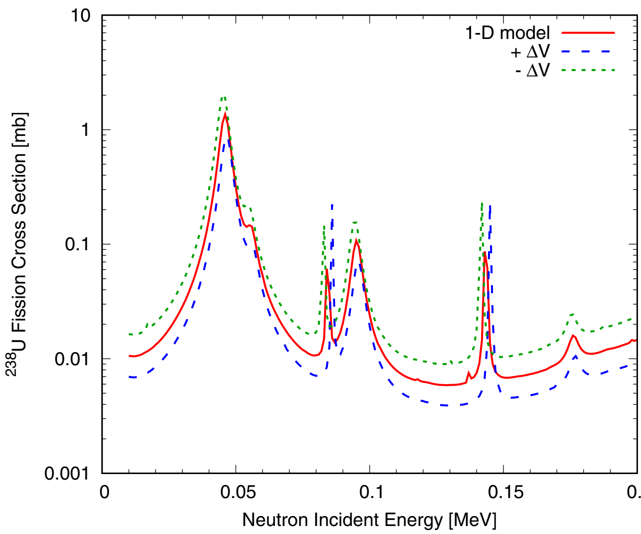

FIG. 6. Calculated fission cross section for neutron-induced reaction on ^{238}U. The barrier height parameters are $V_1 = 6.0$, $V_2 = 0.5$, and $V_3 = 5.0$, the same as in Fig. 5, but a small perturbation $\pm\Delta V$ is applied to the 1-D potential energy surface.

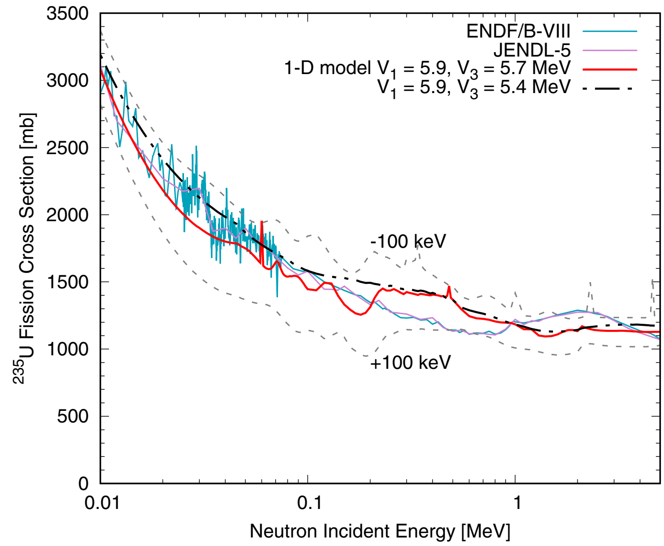

FIG. 7. Calculated fission cross section for neutron-induced reaction on ^{235}U. The barrier height parameters are $V_1 = 5.9$, $V_2 = 0.5$, and $V_3 = 5.7$ MeV for the solid curve. The dashed curves are the case when $V_1 \pm 100$ keV.

reproduces the evaluated fission cross section in the energy range of our interest. The compression parameters $f_0 = 0.8$ and $f_1 = 0.2$ MeV^{-1} were needed to reproduce the fission cross section plateau above 2 MeV. We also calculated the $V_3 = 5.5$ MeV case, which produces a more resonance-like structure below 1 MeV, despite the fact that it tends to underestimate the evaluations on average.

Since the resonating behavior seen in the subthreshold region originates from the wave function in between the inner and outer barriers, their locations and amplitudes strongly depend on the shape of the potential energy surface. Because the 1-D potential energy constructed by smoothly concatenating segmented parabolas is a crude approximation to describe the location of resonances, we naturally understand that such a structure in the experimental data cannot be predicted correctly by the model unless we modify the potential shape freely. That being said, the fission cross sections calculated with the 1-D model in the subthreshold region are not so far from reality, which is usually not so obvious in the T_f^{STD} case. Note that, in evaluated files, resonant structures are usually obtained by adjusting the energy, spin, and parities of class-II states to fit data.

In order to show a sensitivity of the resonance location to the potential shape, we calculated the fission cross sections when the potential energy surface is slightly modified by $\pm\Delta V(x)$, where we adopted a Gaussian form for the perturbation,

$$\Delta V(x) = p_1 \exp\left\{-\frac{(x-p_2)^2}{2p_3^2}\right\}. \tag{20}$$

By setting $p_1 = 0.1$ MeV, $p_2 = 0.3$, and $p_3 = 0.05$, the parabolic shape near the peak of the inner barrier is perturbed by ± 100 keV. The calculated fission cross sections below 200 keV are shown in Fig. 6. A small increase (decrease) in the inner barrier shifts the resonances to the higher (lower) side, which is caused by the phase shift of wave functions.

The neutron-induced reaction on ^{235}U does not have a threshold in the fission channel. The compound nucleus of ^{236}U has the excitation energy of $E_n + S_n = E_n + 6.55$ MeV, and it already has enough energy to fission even for a thermal-energy neutron incident. We adopt the same trajectory compression parameter, V_2, and curvature parameters as those in the ^{238}U calculation, and just look for V_1 and V_3. We found that the set of $V_1 = 5.9$ and $V_3 = 5.7$ MeV gives a reasonable fit to the experimental ^{235}U fission cross section, as compared with the evaluated values in Fig. 7. The resonance-like structure, which is seen in the subthreshold fission of ^{238}U, is also seen near 60 keV. The evaluated data also show a small bump near 30 keV, which might be attributed to enhancement of the wave-function amplitude in between the barriers. However, it is hard to claim that our predicted peak at 60 keV corresponds to the observed bump, as the potential energy shape is oversimplified in this study.

To show a sensitivity of the inner barrier (or the higher one), a range of calculated fission cross sections by changing V_1 by ± 100 keV is shown by the dashed curves. A more resonance-like structure appears when V_1 is reduced to 5.8 MeV, because there is only a 100 keV difference between V_1 and V_3. When the difference is larger, $V_1 + 100$ keV, the structure becomes less pronounced. A similar sensitivity study was performed by Neudecker *el al.* [41], where a 100–150 keV change in the fission barrier height changes the calculated fission cross sections by 10% or so, while the cross-section shape remains the same in the conventional fission model.

While V_1 has such a large sensitivity, the outer barrier (or the lower one) does not change the calculated fission cross section much, as far as V_3 is lower than V_1 by a few hundred keV or more. Figure 7 includes the case of $V_1 = 5.9$ and

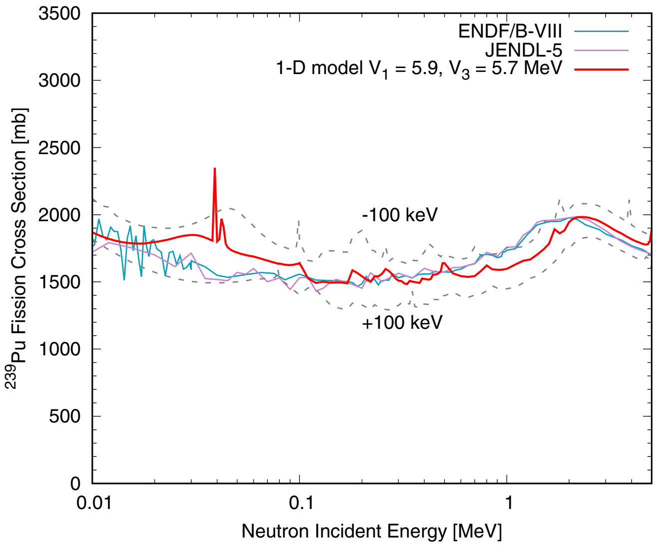

FIG. 8. Calculated fission cross section for neutron-induced reaction on ^{239}Pu. The barrier height parameters are $V_1 = 5.9$, $V_2 = 0.5$, and $V_3 = 5.7$ MeV for the solid curve. The dashed curves are the case when $V_1 \pm 100$ keV.

$V_3 = 5.4$ MeV, where the resonance-like structure is fully washed out. We do not show the sensitivity of V_3 by further lowering the outer barrier, since these curves are hard to distinguish anymore. Astonishingly, the calculated fission cross sections remain almost identical even if $V_3 = 1$ MeV, which implies that the fission calculation is totally governed by the single-humped fission barrier shape.

Figure 8 shows the calculated fission cross section of ^{239}Pu. In this case, it was difficult to obtain a reasonable fit to the evaluations by employing the same compression parameters, and a reduction of f_0 to 0.55 was needed (f_1 is the same as before). The barrier height parameters are $V_1 = 5.9$ and $V_2 = 5.7$ MeV. The resonance-like structure also appears, although it is not as noticeable as in the ^{238}U case. We also show the cross-section band when $V_1 \pm 100$ keV. The sensitivity of V_1 to the fission cross section is similar to ^{235}U. The evaluated cross sections are roughly covered by the ± 100 keV band. However, again, we emphasize that the objective of the present study is not to fit perfectly the model calculation to the experimental data but to demonstrate the fact that the simple 1-D model is potentially capable of capturing the gross features of the fission reaction process by producing calculated fission cross sections in reasonable agreement with experimental data, without the need for a large number of fitting model parameters.

C. Possible refinements

Although we employed the parametrized potential shape, which is constructed using segmented parabolas, the experimental fission cross sections are reasonably reproduced by a few model parameters that characterize the shape itself. This is already a significant improvement of the statistical Hauser-Feshbach calculations for fission compared to the traditional fission calculation by employing $T_f^{\rm STD}$. For better reproduction of available experimental data, as well as prediction of unknown fission cross sections, we envision further improvement by incorporating a few theoretical ingredients.

First, the potential energy shape could be taken from the potential energy surface calculated microscopically [42] or by semimicroscopic approaches [21,43–45]. Because the potential energy surface is often defined in a multidimensional deformation coordinate space, either we have to project the surface onto a one-dimensional axis (it is, however, known that the projection often causes discontinuity problems [46]), or our 1-D model should be extended to a set of coupled equations for the multidimensional coordinate. Second, we should employ a better trajectory compression model rather than the simple damping of Eq. (17), where the nuclear deformation effect is ignored, since it is known that the single-particle spectrum depends on the nuclear deformation. Because our trajectory compression model is constant along the deformation axis, the potential penetration calculation becomes invariant for exchange of the inner and outer barriers, while the calculated potential energy surface often indicates that the inner barrier tends to be higher than the outer barrier for the U and Pu isotopes. Such a property might be seen by introducing the trajectory distortion that is deformation dependent. The nuclear deformation can be calculated with the full- or semimicroscopic approaches, where broken symmetries in the nuclear shape are naturally taken into account. We could also estimate possible trajectories by calculating the microscopic level densities based on the single-particle energies in the deformed one-body potential.

IV. CONCLUSION

We proposed a new model to calculate fission cross sections in the statistical Hauser-Feshbach framework. Instead of applying the WKB approximation for uncoupled fission barriers, as often done in the past, we solved the Schrödinger equation for a one-dimensional (1-D) potential model to calculate the penetration probabilities (transmission coefficients) in the fission channel of compound nucleus reactions. Because we took continuity of the fission path into consideration, the traditional expression to combine several penetrabilities for different barriers, like $T = T_A T_B/(T_A + T_B)$, is no longer involved in our model. Although the potential shape was parameterized by smoothly concatenated parabolas for the sake of convenience, the model can be applied to any arbitrary shape, as we obtain the wave function by the numerical integration technique. This was shown by adding a Gaussian perturbation to the potential shape.

We showed that a resonance structure manifests in the calculated transmission coefficients for the double-humped fission barrier that includes a potential well between them, which is understood to be a quantum mechanical effect in the fission channel. The resonance structure becomes more remarkable when these barriers have a similar height, where the penetration and reflection waves are in phase.

The 1-D potential model was incorporated into the statistical Hauser-Feshbach model to calculate neutron-induced reactions on ^{235,238}U and ^{239}Pu. In order to calculate the potential penetration for the excited states, we introduced a simple trajectory compression model to account for change in the nuclear structure due to the nuclear deformation. By aggregating the fission transmission coefficients for all the possible fission paths, calculated fission cross sections for ^{235,238}U and ^{239}Pu were compared with the evaluated data that represent the experimental cross sections. We showed that reasonable reproduction of the data can be obtained by a limited number of model parameters. Although the detailed structure seen in the experimental fission cross section is hardly reproduced by the 1-D model due to the crude approximation of the adopted potential, further improvement could be made by more careful studies of the potential shape, together with more realistic trajectory compression models.

ACKNOWLEDGMENTS

T.K. thanks B. Morillon and P. Romain of CEA for valuable discussions on this subject. T.K. and P.T. were supported by the Advanced Simulation and Computing (ASC) Program, National Nuclear Security Administration, U.S. Department of Energy. This work was carried out under the auspices of the National Nuclear Security Administration of the U.S. Department of Energy at Los Alamos National Laboratory under Contract No. 89233218CNA000001.

[1] W. Hauser and H. Feshbach, The inelastic scattering of neutrons, Phys. Rev. **87**, 366 (1952).
[2] S. Bjørnholm and J. E. Lynn, The double-humped fission barrier, Rev. Mod. Phys. **52**, 725 (1980).
[3] C. Wagemans, *The Nuclear Fission Process* (CRC, Boca Raton, 1991)
[4] P. Talou and R. Vogt, *Nuclear Fission, Theories, Experiments and Applications* (Springer, Berlin, 2023).
[5] D. L. Hill and J. A. Wheeler, Nuclear constitution and the interpretation of fission phenomena, Phys. Rev. **89**, 1102 (1953).
[6] B. B. Back, O. Hansen, H. C. Britt, and J. D. Garrett, Fission of doubly even actinide nuclei induced by direct reactions, Phys. Rev. C **9**, 1924 (1974).
[7] J. E. Lynn and B. B. Back, Sub-barrier fission probability for a double-humped barrier, J. Phys. A **7**, 395 (1974).
[8] B. B. Back, H. C. Britt, O. Hansen, B. Leroux, and J. D. Garrett, Fission of odd-*A* and doubly odd actinide nuclei induced by direct reactions, Phys. Rev. C **10**, 1948 (1974).
[9] O. Bouland, J. E. Lynn, and P. Talou, *R*-matrix analysis and prediction of low-energy neutron-induced fission cross sections for a range of Pu isotopes, Phys. Rev. C **88**, 054612 (2013).
[10] B. S. Bhandari, Three-hump fission barrier in ^{232}Th, Phys. Rev. C **19**, 1820 (1979).
[11] M. Sin, R. Capote, A. Ventura, M. Herman, and P. Obložinský, Fission of light actinides: ^{232}Th(n, f) and ^{231}Pa(n, f) reactions, Phys. Rev. C **74**, 014608 (2006).
[12] M. Sin, R. Capote, M. W. Herman, and A. Trkov, Extended optical model for fission, Phys. Rev. C **93**, 034605 (2016).
[13] P. Romain, B. Morillon, and H. Duarte, Bruyères-le-Châtel neutron evaluations of actinides with the TALYS code: The fission channel, Nucl. Data Sheets **131**, 222 (2016), Special Issue on Nuclear Reaction Data.
[14] J. D. Cramer and J. R. Nix, Exact calculation of the penetrability through two-peaked fission barriers, Phys. Rev. C **2**, 1048 (1970).
[15] R. C. Sharma and J. N. Leboeuf, Three-hump potential barrier in the ^{234}Th nucleus, Phys. Rev. C **14**, 2340 (1976).
[16] B. Morillon, H. Duarte, and P. Romain, Petits problèmes de transmission quantique, CEA Technical Report, 2010 (unpublished).
[17] T. Kawano, Exact solution of fission penetration through arbitrary complex fission barrier, Los Alamos National Laboratory Technical Report No. LA-UR-15-24956, 2015 (unpublished).
[18] A. Junghans, M. de Jong, H.-G. Clerc, A. Ignatyuk, G. Kudyaev, and K.-H. Schmidt, Projectile-fragment yields as a probe for the collective enhancement in the nuclear level density, Nucl. Phys. A **629**, 635 (1998).
[19] O. Iwamoto, Development of a comprehensive code for nuclear data evaluation, CCONE, and validation using neutron-induced cross sections for uranium isotopes, J. Nucl. Sci. Technol. **44**, 687 (2007).
[20] J. R. Nix, Further studies in the liquid-drop theory on nuclear fission, Nucl. Phys. A **130**, 241 (1969).
[21] P. Möller, A. J. Sierk, T. Ichikawa, A. Iwamoto, R. Bengtsson, H. Uhrenholt, and S. Åberg, Heavy-element fission barriers, Phys. Rev. C **79**, 064304 (2009).
[22] B. B. Back, J. P. Bondorf, G. A. Otroschenko, J. Pedersen, and B. Rasmussen, Fission of U, Np, Pu and Am isotopes excited in the (d,p) reaction, Nucl. Phys. A **165**, 449 (1971).
[23] L. Fox and E. T. Goodwin, Some new methods for the numerical integration of ordinary differential equations, Math. Proc. Cambridge Philos. Soc. **45**, 373 (1949).
[24] S. Hilaire, C. Lagrange, and A. J. Koning, Comparisons between various width fluctuation correction factors for compound nucleus reactions, Ann. Phys. (NY) **306**, 209 (2003).
[25] E. V. Gai, A. V. Ignatyuk, N. Srabotnov, and G. N. Smirenkin, Double hump barrier in the quasiclassical approaching, in *Proceedings of the IAEA Symposium on Physics and Chemistry of Fission, IAEA-SM-122/132* (International Atomic Energy Agency, Vienna, 1969), pp. 337–347, in Russian.
[26] T. Kawano, CoH$_3$: The coupled-channels and Hauser-Feshbach code, in *CNR2018: International Workshop on Compound Nucleus and Related Topics*, LBNL, Berkeley, September 24–28, 2018, edited by J. Escher, Y. Alhassid, L.A. Bernstein, D. Brown, C. Fröhlich, P. Talou, and W. Younes, Proceedings in Physics Vol. 254 (Springer, Berlin, 2021), p. 27.
[27] C. A. Engelbrecht and H. A. Weidenmüller, Hauser-Feshbach theory and ericson fluctuations in the presence of direct reactions, Phys. Rev. C **8**, 859 (1973).
[28] T. Kawano, P. Talou, and H. A. Weidenmüller, Random-matrix approach to the statistical compound nuclear reaction at low energies using the Monte Carlo technique, Phys. Rev. C **92**, 044617 (2015).
[29] T. Kawano, R. Capote, S. Hilaire, and P. Chau Huu-Tai, Statistical Hauser-Feshbach theory with width-fluctuation correction including direct reaction channels for neutron-induced reactions at low energies, Phys. Rev. C **94**, 014612 (2016).

[30] G. R. Satchler, Average compound nucleus cross sections in the continuum, Phys. Lett. **7**, 55 (1963).
[31] E. S. Soukhovitskii, S. Chiba, J.-Y. Lee, O. Iwamoto, and T. Fukahori, Global coupled-channel optical potential for nucleon-actinide interaction from 1 keV to 200 MeV, J. Phys. G: Nucl. Part. Phys. **30**, 905 (2004).
[32] T. Kawano, P. Talou, J. E. Lynn, M. B. Chadwick, and D. G. Madland, Calculation of nuclear reaction cross sections on excited nuclei with the coupled-channels method, Phys. Rev. C **80**, 024611 (2009).
[33] J. Kopecky and M. Uhl, Test of gamma-ray strength functions in nuclear reaction model calculations, Phys. Rev. C **41**, 1941 (1990).
[34] M. R. Mumpower, T. Kawano, J. L. Ullmann, M. Krtička, and T. M. Sprouse, Estimation of $M1$ scissors mode strength for deformed nuclei in the medium- to heavy-mass region by statistical Hauser-Feshbach model calculations, Phys. Rev. C **96**, 024612 (2017).
[35] A. Gilbert and A. G. W. Cameron, A composite nuclear-level density formula with shell corrections, Can. J. Phys. **43**, 1446 (1965).
[36] T. Kawano, S. Chiba, and H. Koura, Phenomenological nuclear level densities using the KTUY05 nuclear mass formula for applications off-stability, J. Nucl. Sci. Technol. **43**, 1 (2006).
[37] R. Capote, M. Herman, P. Obložinský, P. G. Young, S. Goriely, T. Belgya, A. V. Ignatyuk, A. J. Koning, S. Hilaire, V. A. Plujko, M. Avrigeanu, O. Bersillon, M. B. Chadwick, T. Fukahori, Z. Ge, Y. Han, S. Kailas, J. Kopecky, V. M. Maslov, G. Reffo *et al.*, RIPL - Reference Input Parameter Library for calculation of nuclear reactions and nuclear data evaluations, Nucl. Data Sheets **110**, 3107 (2009).
[38] P. Möller, J. R. Nix, W. D. Myer, and W. J. Swiatecki, Nuclear ground-state masses and deformations, At. Data Nucl. Data Tables **59**, 185 (1995).
[39] D. A. Brown, M. B. Chadwick, R. Capote, A. C. Kahler, A. Trkov, M. W. Herman, A. A. Sonzogni, Y. Danon, A. D. Carlson, M. Dunn, D. L. Smith, G. M. Hale, G. Arbanas, R. Arcilla, C. R. Bates, B. Beck, B. Becker, F. Brown, R. J. Casperson, J. Conlin *et al.*, ENDF/B-VIII.0: the 8th major release of the nuclear reaction data library with CIELO-project cross sections, new standards and thermal scattering data, Nucl. Data Sheets **148**, 1 (2018).
[40] O. Iwamoto, N. Iwamoto, S. Kunieda, F. Minato, S. Nakayama, Y. Abe, K. Tsubakihara, S. Okumura, C. Ishizuka, T. Yoshida, S. Chiba, N. Otuka, J.-C. Sublet, H. Iwamoto, K. Yamamoto, Y. Nagaya, K. Tada, C. Konno, N. Matsuda, K. Yokoyama *et al.*, Japanese evaluated nuclear data library version 5: JENDL-5, J. Nucl. Sci. Technol. **60**, 1 (2023).
[41] D. Neudecker, O. Cabellos, A. R. Clark, M. J. Grosskopf, W. Haeck, M. W. Herman, J. Hutchinson, T. Kawano, A. E. Lovell, I. Stetcu, P. Talou, and S. V. Wiel, Informing nuclear physics via machine learning methods with differential and integral experiments, Phys. Rev. C **104**, 034611 (2021).
[42] S. Goriely, S. Hilaire, A. J. Koning, M. Sin, and R. Capote, Towards a prediction of fission cross sections on the basis of microscopic nuclear inputs, Phys. Rev. C **79**, 024612 (2009).
[43] P. Möller and J. Randrup, Calculated fission-fragment yield systematics in the region $74 \leqslant Z \leqslant 94$ and $90 \leqslant N \leqslant 150$, Phys. Rev. C **91**, 044316 (2015).
[44] M. Verriere and M. R. Mumpower, Improvements to the macroscopic-microscopic approach of nuclear fission, Phys. Rev. C **103**, 034617 (2021).
[45] P. Jachimowicz, M. Kowal, and J. Skalski, Properties of heaviest nuclei with $98 \leqslant Z \leqslant 126$ and $134 \leqslant N \leqslant 192$, At. Data Nucl. Data Tables **138**, 101393 (2021).
[46] N. Dubray and D. Regnier, Numerical search of discontinuities in self-consistent potential energy surfaces, Comput. Phys. Commun. **183**, 2035 (2012).